JOURNAL OF THE KOREAN ASTRONOMICAL SOCIETY
38: 129 ~ 132, 2005

INTERGALACTIC MEDIUM IN THE ΛCDM UNIVERSE FROM COSMOLOGICAL SIMULATIONS

LONG-LONG FENG[1], PING HE, LIZHI FANG[2], CHI-WANG SHU[3], MENG-PING ZHANG[4]
[1]Purple Mountain Observatory, Nanjing, 210008, P.R.China
E-mail: fengll@pmo.ac.cn
[2]Department of Physics, University of Arizona, Tucson, AZ 85712, USA
[3]Division of Applied Mathematics, Brown University, Providence, RI 02912,U.S.A.
[4]Department of Mathematics, University of Science and Technology of China,
Anhui, Hefei, 230026, P.R. China
(Received February 1, 2005; Accepted March 15, 2005)

ABSTRACT

The temperature (T) and entropy (S) fields of baryonic gas, or intergalactic medium (IGM), in the ΛCDM cosmology are analyzed using simulation samples produced by a hybrid cosmological hydrodynamic/N-body code based on the weighted essentially non-oscillatory scheme. We demonstrate that , in the nonlinear regime, the dynamical similarity between the IGM and dark matter will be broken in the presence of strong shocks in the IGM. The heating and entropy production by the shocks breaks the IGM into multiple phases. The multiphase and non-Gaussianity of the IGM field would be helpful to account for the high-temperature and high-entropy gas observed in groups and clusters with low-temperature IGM observed by Lyα forest lines and the intermittency observed by the spikes of quasi-stellar object's absorption spectrum.

Key words : cosmology: theory - intergalactic medium - large-scale structure of the universe - methods: numerical

I. INTRODUCTION

The standard paradigm for the formation of cosmic large-scale structures in the universe is the hierarchical clustering scenario. This scenario assumes that massive dark matter halos are formed via the processes of gravitational collapse, merging of smaller structures, and accretion. Light-emitting and -absorbing objects form when the baryonic gas, i.e., the intergalactic medium (IGM), falls, cools, and condenses around and within the dark halos. The evolution of the IGM in this model is largely determined by the underlying dark matter. It is usually assumed that the dynamical behavior of the IGM field can be obtained from the dark matter field by a similarity mapping between them on scales larger than the Jeans length scales (Bi et al. 1992; Fang et al. 1993; Nusser & Haehnelt 1999).

The similarity mapping works in linear regime. However, entering into the nonlinear regime, this kind of similarity may not always be present. The dynamical mechanism of violating the similarity between the IGM and dark matter has been discussed in the early study of structure formation (Shandarin & Zel'dovich 1989). As the dark matter particles are collisionless, the velocity of the dark matter particles will be multivalued at the intersection of the dark matter particle trajectories; while for the IGM, its velocity field is single-valued everywhere. Thus, at the intersection of the dark matter particle trajectories, the density of gas would be discontinuous, and shocks or complex structures occur. The development of shocks or complex structures breaks the similarity between the IGM and dark matter and thus leads to the statistical discrepancy between the IGM distribution and dark matter mass field.

Moreover, strong shocks and complex structures result in the heating and the entropy increase of the IGM. The cosmic baryonic gas involved in strong shocks should hence undergo an entropy increase. The dark matter remains unaffected. Consequently, the IGM will be in thermodynamically multiple phases. The relations between the temperature and mass density, or entropy and mass density of the IGM will not be described by an single-value relation and will vary from place to place(He et al, 2004). This paper is going to focus on the temperature and entropy fields of the IGM based on the cosmological hydrodynamic simulations and its cosmological implication.

II. COSMOLOGICAL HYDRODYNAMIC SIMULATIONS

We developed a hybrid N-body/hydrodynamical code that incorporates a Lagrangian particle-mesh algorithm to evolve the collision-less matter with the fifth order weighted essentially non-oscillatory scheme (WENO) to solve the equation of gas dynamics (Jiang & Shu, 1996; Shu, 1998, Feng et.al, 2004). WENO realizes the

Proceedings of *the 6th East Asian Meeting of Astronomy*, held at Seoul National University, Korea, from October 18-22, 2004.

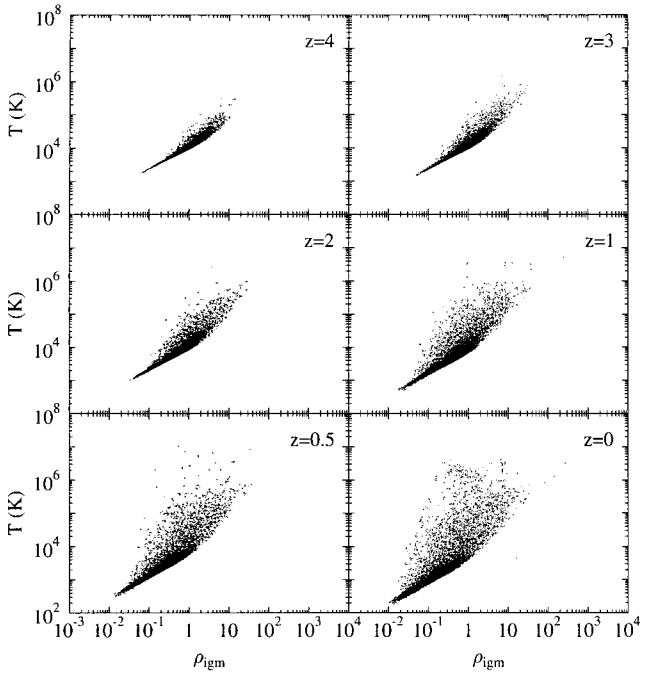

Fig. 1.— Temperature T vs. IGM density ρ_{igm}. Each panel is given by 19,200 points randomly drawn from the simulation sample in $25^3 h^{-3}$ Mpc^3 box with 192^3 data points

idea of adaptive stencils in the reconstruction procedure based on the local smoothness of the numerical solution to automatically achieve high order accuracy and non-oscillatory property near discontinuities. It is extremely robust and stable for solutions containing strong shock and complex solution structures.

In the present application, we computed the cosmic evolution of the coupled system of both dark matter and baryonic matter in a flat low density CDM model (ΛCDM), which is specified by the density parameter $\Omega_m = 0.3$, cosmological constant $\Omega_\Lambda = 0.7$, Hubble constant $h = 0.7$, and mass fluctuation within a sphere of radius $8h^{-1}$Mpc, $\sigma_8 = 0.9$. We perform the simulations in a 192^3 grid with an equal number of dark matter particles. Atomic processes including ionization, radiative cooling and heating are modeled as in Cen (1992) in a primeval plasma of hydrogen and helium of composition ($X = 0.76$, $Y = 0.24$). The uniform UV-background of ionizing photons is assumed to have a power-law spectrum of the form $J(\nu) = J_{21} \times 10^{-21}(\nu/\nu_{HI})^{-\alpha}$ergs^{-1}cm^{-2}sr^{-1}Hz^{-1}, where the photoionizing flux is normalized by parameter J_{21} at the Lyman limit frequency ν_{HI}, and is suddenly switched on at $z \sim 6$ to heat the gas and reionize the universe.

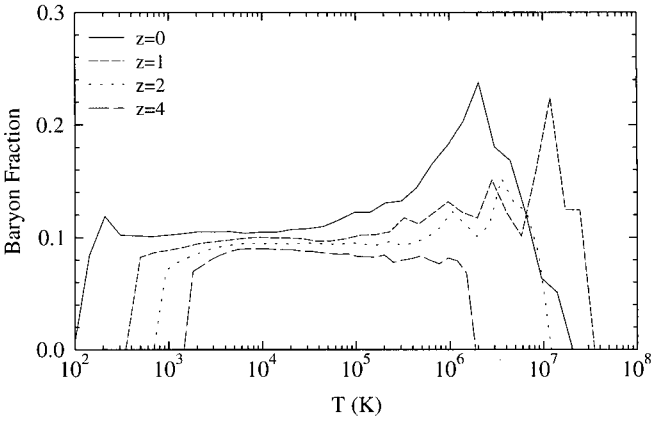

Fig. 2.— Relations of the mean baryonic fraction with respect to temperature of the IGM. The redshifts are taken to be 4.0, 2.0, 1.0, and 0.

III. MULTIPLE PHASES IN THE TEMPERATURE-DENSITY DIAGRAM

In Figure 1 we show the relations between the temperature and mass density of the IGM at z =4, 3, 2, 1, 0.5, and 0.0. The basic feature of the $T - \rho_{igm}$ diagram looks similar to those given by other cosmological hydrodynamic simulations or semi-analytical models (e.g., Ryu et al. 1993; Katz et al. 1996; Theuns et al. 1998; Davé et al. 1999; Valageas et al. 2002; Springel & Hernquist 2002). Roughly speaking, there are two phases in the $T-\rho_{igm}$ plane. (1) The first phase manifests a tight correlation in the bottom left regions T ($\leq 10^{4.5}$K) and $0.01 < \rho_{igm} < 2$, and (2) the second phase lies above the tight correlation regions and has a scattered distribution in which the temperature generally is greater than 10^5K.

The tight correlation lines can be well approximated by a power law as $T \propto \rho_{igm}^{\alpha}$ with α slightly increasing from $\sim$0.61 at z=4 to $\sim$0.69 at z=0, which is the same as the so-called IGM equation of state given by Hui & Gnedin (1997). The small discrepancy of α from the adiabatic index $\gamma - 1 = 2/3$ results from the photoionization heating and radiative cooling (Valageas et al. 2002).

The gas in phase 2 sometimes is called the warm-hot intergalactic medium (WHIM), as its temperature is $\sim 10^5 - 10^7$ K, i.e., higher than the gas in phase 1 by a factor of about $10 - 10^3$ (Cen & Ostriker 1999). From Figure 1 we can see that the WHIM underwent a significant evolution from redshift $z = 4$ to the present. At $z = 4$ WHIM events are rare and mostly reside in the regions of mass density, $\rho_{igm} \geq 1$, while WHIM becomes quite common when $z \leq 2$. Note that the high-temperature ($10^6 - 10^7$ K) events, and hence strong shocks, can also occur in the regions with density $\rho_{igm} \sim 1$, and even $\rho_{igm} \simeq 0.1$.

The relationships between the mean baryonic fraction and temperature is displayed in Figure 2. It is obvious that the baryon fraction at $z \leq 1$ significantly exceeds the cosmological value f_b for the WHIM (at $10^5\mathrm{K} < T < 10^7$ K). This is a well-known result nowadays (Cen & Ostriker 1999; Davé et al. 2001). The concentration of baryons into WHIM can be seen as follows. The gas is compressed by a factor of ~ 4 by strong shocks. On the other hand, the dark matter mass density at the pre- and postshock is almost the same. Thus, the baryon fraction in the postshocked IGM can be enhanced as high as $4 \times 0.085 \simeq 0.3$.

The entropy of the IGM is measured by the parameter $T/n_{igm}^{2/3}$, where n_{igm} is the number density of baryons. It is actually related to the entropy density s of the IGM by $s/\rho_{igm} = \ln T/n_{igm}^{2/3} +$ const. As we will not use s below, we use this notation for the entropy parameter or simply entropy, $S = T/n_{igm}^{2/3}$. If temperature T is in units of keV (1 keV $\simeq 1.2 \times 10^7$ K), entropy S is in units of keV cm^2. Figure 3 presents the relation between the entropy and temperature of the IGM at redshifts $z = 4$, 3, 2, 1, 0.5, and 0.

Figure 3 also indicates the two phases of the IGM: (1) a tight correlation along a line of $S \simeq$ const at the bottom of the figure, i.e., the entropy of the IGM is independent of IGM temperature, and (2) a scattered distribution above the tight correlation line. It is consistent with Figure 1. The gas in phase 1 approximately satisfies $T \propto \rho_{igm}^{2/3}$. The gas in phase 2 experiences an entropy increase process, mainly because of the heating by shocks in the IGM. A strong shock increases T by a factor of $10^1 - 10^3$, n_{igm} by a factor of $\sim$4, and therefore, the postshocked entropy can be enhanced by a factor of $10^1 - 10^3$.

Phase 2 shows a significant evolution from redshift $z = 4$ to the present. There are almost no high-entropy ($S > 50$ h$^{-1/3}$ keV cm^2) events when $z = 4$. At $z = 2$ and 3, high-entropy events are biased to $T > 5 \times 10^{-3}$ keV regions. When $z \leq 1$, high-entropy events occur in all temperatures $T > 10^{-3}$ keV, or greater than 10^4 K ranges.

Figure 4a presents the mean entropy $\overline{S}$ versus density ρ_{dm}. The entropy of the IGM increases by about 2 orders of magnitude from redshift $z = 4$ to 0.5. In the redshift range $3 > z > 1$, the mean entropy $\overline{S}$ is higher in higher density areas. For dark matter mass density $\rho_{dm} > 10^2$, the mean entropy $\bar{S}$ is greater than 60 h$^{-1/3}$ keV cm^2 at the epoch $z \simeq 2$, and greater than 20 h$^{-1/3}$ keV cm^2 at $z \simeq 3$. At $z \leq 0.5$, the shocks and complicated structures yield an "entropy floor" $\overline{S} \sim 100 - 300\ h^{-1/3}$ keV cm^2 at $z \leq 0.5$ over the entire IGM from low-density ($\rho_{dm} \simeq 10^{-2}$) areas to high-density ($\rho_{dm} \simeq 10^3$) regions. This is the cosmological background of entropy floor generated by the nonlinear evolution of the IGM in the gravity of dark matter (Valageas et al, 2003; He et al, 2004).

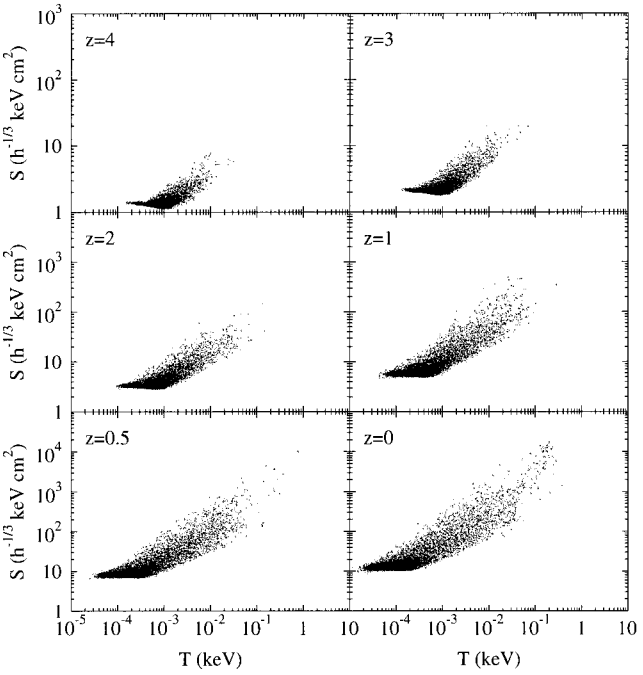

Fig. 3.— Entropy S vs. Temperature T. Each panel is given by 19,200 points randomly drawn from the simulation sample in 25^3 h^{-3} Mpc^3 box with 192^3 data points.

In Figure 4b, we show the $\overline{S}$ - ρ_{igm} relation for samples produced by the same cosmological parameters, but without considering radiative cooling and photoionization heating. We see that the relation $\overline{S}$ - ρ_{igm} at $z \leq 2$ in Figure 4b is about the same as that of Figure 4a, especially in the high-density range ($\rho_{dm} > 10$). Therefore, the entropy increase of the IGM at $z \leq 2$ shown in Figure 4a is not due to the heating and cooling, but mainly determined by shocks and complicated structures. The effects of radiative cooling and heating to the entropy evolution are negligible at $z \leq 2$ and high-density areas. At higher redshift $z > 2$ and low-density areas, however, the effects of radiative cooling and heating become important.

IV. DISCUSSIONS

The multiphased feature and non-Gaussianity of the IGM temperature and entropy fields can effectively be applied to explain the following IGM-related observations.

1. Entropy floor of groups and clusters.—For all regions on scales greater than 1 h^{-1} Mpc and with dark matter mass density $\rho_{dm} > 10^2$, the mean entropy $\bar{S}$, or entropy floor, is greater than 80 $h^{-1/3}$ keV cm^2 since the epoch $z \simeq 2$ and greater than 20 $h^{-1/3}$ keV cm^2 at $z \simeq 3$. Even for regions of $\rho_{dm} > 10$, the mean entropy still have $\bar{S} > 25\ h^{-1/3}$ keV cm^2 at the epoch $z \simeq 2$ and 10 $h^{-1/3}$ keV cm^2 at $z \simeq 3$. Therefore, gravitational shock is an important provider of high-entropy

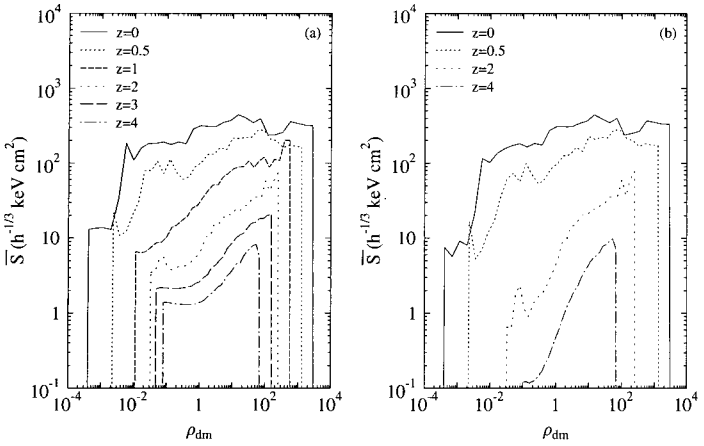

Fig. 4.— Mean entropy $\overline{S}$ vs. ρ_{dm} (a) for the simulation with ionizing, radiation heating, and cooling at redshifts 4.0, 3.0, 2.0, 1.0, 0.5, and 0.0, and (b) for the simulation without ionizing, radiation heating, and cooling at redshifts 4.0, 2.0, 0.5, and 0.0.

gas around massive halos, which are the hosts of clusters and groups. This result is adequate to explain the entropy excess from the observations of clusters and groups if the epoch of the gas falling in cluster cores is not earlier than $z \simeq 2 - 3$ (Ponman et al. 2003). In other words, the IGM is already significantly preheated by gravitational shocks at the epoch $z \simeq 2 - 3$, and therefore other sources of heating may not be important if the cluster core with entropy excess formed after that epoch (Kay & Bower 1999; Borgani et al 2002).

2. Lyα forest lines.—The Lyα forest lines in QSO's absorption spectrum of $2 < z < 4$ have a column density N_{HI} of HI atoms in the range $13 < \ln N_{HI} < 14$, which corresponds to areas of $\rho_{dm} \simeq 1$ (Bi & Davidsen 1997). The thermal broadening of these lines shows that the temperature of the IGM at this density area is about $10^4 - 10^5$K. The high-entropy floor ($S \sim 100h^{-1/3}$ keV cm^2) will contradict the Lyα forest if the entropy field is uniform. However, the temperature and entropy fields are highly non-Gaussian and of multiple phases. The volume of the universe is actually dominated by regions of low temperature and low mass density. For all redshifts $z \leq 4$, more than 90% volume with dark matter mass density ($\rho_{dm} \leq 2$) is occupied by the IGM with temperature less than $10^{4.5}$K. This provides the room for the QSO's Lyα forests. The mean temperature is higher for lower redshifts. Therefore, the number density of the forests lines, or absorbers, is lower at lower redshifts. These properties match the constraints on the IGM from QSO's Lyα forests. Moreover, the non-Gaussianity and multiple phases of the IGM is capable of accounting for the intermittency of Lyα transmitted flux (Jamkhedkar et al, 2002, 2003, Feng et al, 2003).

ACKNOWLEDGEMENTS

This work is supported by the National Science Foundation of China (NSFC 10173009, 10025313,10028103) and the National Key Basic Research Science Foundation (NKBRSF G19990752). CWS also acknowledges support from ARO grant DAAD19-00-1-0405 and NSF grant DMS-0207451.

REFERENCES

Borgani, S., Governato, F., Wadsley, J., Menci, N.,
Tozzi, P., Quinn, T., Stadel, J, & Lake, G. 2002, MNRAS, 336,
409

Bi, H.G., Börner, G., & Chu, Y.Q. 1992, A&A,
266,1

Bi, H.G., & Davidsen, A. F. 1997, ApJ, 479, 523

Cen, R. 1992, ApJS, 78, 341

Cen, R., & Ostriker, J. 1999, ApJ, 514, 1

Davé, R., Cen, R., Ostriker, J., Bryan, G.L.,
Hernquist, L., Katz, N., Weinberg, D.H., Norman, M.L., & O'Shea, B. 2001,
ApJ, 552, 473

Fang, L.Z., Bi, H.G., Xiang, S.P, & Börner, G.
1993, ApJ, 413, 477

Feng, L.L., Pando, J., & Fang, L.Z. 2003, ApJ, 587,
487

Feng, L.L., Shu, C.W., & Zhang, M.P. 2004, ApJ,
612, 1

He, P., Feng, L.L., & Fang, L.Z. 2004, ApJ, 612, 14

Hui, L., & Gnedin, N.Y., 1997, MNRAS, 292, 27

Jamkhedkar, P., Zhan, H., & Fang, L.Z. 2000, ApJ,
543, L1

Jamkhedkar, P., Feng, L.L., Zheng, W., Kirkman, D.,
Tytler, D., & Fang, L.Z. 2003, MNRAS, 343, 1110

Jiang, G., & Shu, C.W. 1996, J. Comput. Phys., 126,
202

Katz, N., Weinberg, D.H., & Hernquist, L. 1996,
ApJS, 105, 19

Kay, S., & Bower, R. 1999, MNRAS, 308, 664

Nusser, A., & Haehnelt, M. 1999, MNRAS, 303, 179

Ponman, T., Sanderson, A., & Finoguenov, A. 2003,
MNRAS, 343, 331

Ryu, D., Ostriker, O., Kang, H., & Cen, R. 1993,
ApJ, 414, 1

Shandarin, S.F., & Zel'dovich, Ya.B. 1989, Rev.
Mod.
Phys., 61, 185

Shu, C.W. 1998, in Advanced Numerical Approximation